



OPEN ACCESS

EDITED BY

Anne Elisabeth Bjune,
University of Bergen, Norway

REVIEWED BY

Barry Alan Gardiner,
Institut Européen De La Forêt Cultivée
(IEFC), France
Katarina Čufar,
University of Ljubljana, Slovenia

*CORRESPONDENCE

J. Julio Camarero

✉ jjcamarero@ipe.csic.es

RECEIVED 22 March 2023

ACCEPTED 24 July 2023

PUBLISHED 14 August 2023

CITATION

Camarero JJ, Colangelo M, Rita A, Hevia A,
Pizarro M and Voltas J (2023) A multi-
proxy framework to detect insect
defoliations in tree rings: a case
study on pine processionary.
Front. Ecol. Evol. 11:1192036.
doi: 10.3389/fevo.2023.1192036

COPYRIGHT

© 2023 Camarero, Colangelo, Rita, Hevia,
Pizarro and Voltas. This is an open-access
article distributed under the terms of the
[Creative Commons Attribution License
\(CC BY\)](https://creativecommons.org/licenses/by/4.0/). The use, distribution or
reproduction in other forums is permitted,
provided the original author(s) and the
copyright owner(s) are credited and that
the original publication in this journal is
cited, in accordance with accepted
academic practice. No use, distribution or
reproduction is permitted which does not
comply with these terms.

A multi-proxy framework to detect insect defoliations in tree rings: a case study on pine processionary

J. Julio Camarero^{1*}, Michele Colangelo^{1,2}, Angelo Rita³,
Andrea Hevia^{4,5}, Manuel Pizarro¹ and Jordi Voltas^{6,7}

¹Instituto Pirenaico de Ecología (IPE-CSIC), Zaragoza, Spain, ²Scuola di Scienze Agrarie, Forestali, Alimentari e Ambientali, Università della Basilicata, Potenza, Italy, ³Dipartimento di Agraria, Università di Napoli Federico II, Napoli, Italy, ⁴DendroOlavide-Dept. Sistemas Físicos, Químicos y Naturales, Universidad Pablo de Olavide, Sevilla, Spain, ⁵Departamento de Biología Animal, Biología Vegetal y Ecología, Universidad de Jaén, Jaén, Spain, ⁶Joint Research Unit CTFC – AGROTECNIO - CERCA, Lleida, Spain, ⁷Department of Agricultural and Forest Sciences and Engineering, Universitat de Lleida, Lleida, Spain

Assessing and reconstructing the impacts of defoliation caused by insect herbivores on tree growth, carbon budget and water use, and differentiating these impacts from other stresses and disturbances such as droughts requires multi-proxy approaches. Here we present a methodological framework to pinpoint the impacts of pine processionary moth (*Thaumetopoea pityocampa*), a major winter-feeding defoliator, on tree cover (remote-sensing indices), radial growth and wood features (anatomy, density, lignin/carbohydrate ratio of cell walls, $\delta^{13}\text{C}$ and $\delta^{18}\text{O}$ of wood cellulose) of drought-prone pine (*Pinus nigra*) forests in north-eastern Spain. We compared host defoliated (D) and coexisting non-defoliated (ND) pines along with non-host oaks (*Quercus faginea*) following a strong insect outbreak occurring in 2016 at two climatically contrasting sites (cool-wet Huesca and warm-dry Teruel). Changes in tree-ring width and wood density were analyzed and their responses to climate variables (including a drought index) were compared between D and ND trees. The Normalized Difference Infrared Index showed reductions due to the outbreak of -47.3% and -55.6% in Huesca and Teruel, respectively. The D pines showed: a strong drop in growth (-96.3% on average), a reduction in tracheid lumen diameter (-35.0%) and lower lignin/carbohydrate ratios of tracheid cell-walls. Both pines and oaks showed synchronous growth reductions during dry years. In the wet Huesca site, lower wood $\delta^{13}\text{C}$ values and a stronger coupling between $\delta^{13}\text{C}$ and $\delta^{18}\text{O}$ were observed in D as compared with ND pines. In the dry Teruel site, the minimum wood density of ND pines responded more negatively to spring drought than that of D pines. We argue that multi-proxy assessments that combine several variables have the potential to improve our ability to pinpoint and reconstruct insect outbreaks using tree-ring data.

KEYWORDS

outbreak, *Pinus nigra*, Raman spectroscopy, *Thaumetopoea pityocampa*, wood anatomy, wood isotopes

1 Introduction

Insect herbivores are important forest stressors that are becoming increasingly relevant under ongoing climate warming (Ayres and Lombardero, 2000) and forest expansion (Azcárate et al., 2023). Climate- and human-mediated range expansions of herbivore insects are altering their impacts on forests (Simler-Williamson et al., 2019). For instance, higher temperatures can enhance reproduction rates promoting the dispersal of insect herbivores whose distributions are limited by cold winters (Harvey et al., 2020). In Mediterranean conifer forests, a widely reported case of range expansion linked to rising winter temperatures is the pine processionary moth (*Thaumetopoea pityocampa* Den. & Schiff., Lepidoptera: Thaumetopoeidae; hereafter abbreviated as PPM), a major defoliator of drought-prone pine and cedar stands (Roques et al., 2015). The PPM population dynamics follows a positive gradation phase until maximum PPM density is reached, then crown defoliation levels peak in the outbreak maximum with PPM density and decreases afterwards due to reduced food availability (Démolin, 1969; Battisti et al., 2005; Battisti et al., 2015). Since PPM moths feed on conifer needles within silky nests, and low winter temperatures limit the development of PPM moths (Démolin, 1969; Roques et al., 2015), recent upward or poleward expansions of PPM in some places have been attributed to warmer winter conditions (Hóðar et al., 2003, 2004). The PPM causes defoliation of pine and cedar forests across the Mediterranean Basin, particularly affecting stands of species such as black pine (*Pinus nigra* J.F. Arn.), Scots pine (*Pinus sylvestris* L.), Aleppo pine (*Pinus halepensis* Mill) and maritime pine (*Pinus pinaster* Ait.), while others such as stone pine (*Pinus pinea* L.) are less affected (Gazol et al., 2019; Azcárate et al., 2023).

Forests are not exclusively impacted by single factors; rather, disturbances and/or stressors interact reducing forest productivity and modifying forest dynamics (Millar and Stephenson, 2015). For instance, rising winter temperatures may enhance PPM impacts on Mediterranean conifers but also amplify drought stress, making trees more vulnerable to insect damage by reducing radial growth, increasing defoliation and enhancing tree mortality risk (Jactel et al., 2012). However, it is still unknown how stressors such as PPM defoliations and drought interact and affect long-term Mediterranean conifer forest dynamics (Linares et al., 2014; Camarero et al., 2022a). To answer this question, tree-ring based reconstructions of insect outbreaks together with geographically detailed and temporally updated field reports of related defoliation are needed (Sangüesa-Barreda et al., 2014; Navarro et al., 2018; Gazol et al., 2019).

In order to perform dendrochronological reconstructions of insect outbreaks, standardized tree-ring width series from coexisting host and non-host tree species showing similar responses to climate or drought severity can be compared (Swetnam et al., 1985; Swetnam and Lynch, 1993; Speer et al., 2001; Paritsis et al., 2009; Lynch, 2012). However, differentiating the negative impacts of severe defoliation and drought on radial growth is not always straightforward, because these stressors can show different carry-over (legacy) effects (Sangüesa-Barreda et al., 2014; Camarero et al., 2022a). An exception would be tree rings showing wood-anatomical signatures of insect defoliation such as white rings with xylem cells

showing a low lignification degree (Sutton and Tardif, 2005), but these markers of outbreaks are not frequently observed. In the case of drought, conifers often show reduced earlywood production and a higher minimum wood density related to tracheids with narrow lumen (Camarero et al., 2014; Camarero et al., 2015; Camarero and Hevia, 2020; Camarero et al., 2021).

It is assumed that the magnitude of radial growth reduction is proportional to the amount of foliage removed by insect herbivores, albeit this relationship may be asymptotic (Kulman, 1971; Gross, 1992). This is also the case of PPM outbreaks in Mediterranean conifer forests (Hóðar et al., 2003; Hóðar et al., 2004; Battisti et al., 2015; Gazol et al., 2019). Several studies in particular have demonstrated that PPM outbreaks associated with high defoliation levels cause severe reductions in radial growth (Hernández Alonso et al., 2005; Kanat et al., 2005; Camarero et al., 2022a). The relative loss in radial growth due to PPM outbreaks depended on defoliation degree, with low (< 25%) and severe defoliation levels (> 50%) inducing growth losses of 20% and 50%, respectively (Jacquet et al., 2012). According to Polge and Garros (1971), PPM defoliation not only reduces tree-ring width but also earlywood density through the formation of tracheids with thin cell walls (with a reduction of 35.0% on average), but with normal lumen diameters. However, the impacts of PPM defoliation on tree growth and wood anatomy have not been further assessed by comparing several measures of insect impact.

In this study, we applied a multi-proxy approach to identify the impacts of PPM severe defoliations on forest cover based on remote-sensing, radial growth, and carbon and water use data. We analyzed several xylem features (wood density, wood anatomy variables such as lumen diameter and cell-wall thickness, C and O isotope composition, lignification degree of tracheid cell-walls), which are proxies of carbon use in tracheid walls building (e.g., wood density) and intrinsic water-use efficiency (e.g., cellulose $\delta^{13}\text{C}$). First, we followed the classical tree-ring approach by comparing the growth of defoliated host species (*Pinus nigra*) with that of coexisting, non-defoliated trees of the same species and also of a different non-host (non-defoliated) species (*Quercus faginea*). Second, to pinpoint the impact of a severe PPM defoliation we analyzed changes in forest cover using remote sensing indices, and compared growth (tree-ring width) and wood features (density and tracheid anatomy, C and O isotope composition, lignification degree of cell walls) between severely defoliated pines and non-defoliated pines and oaks. We hypothesized that the PPM outbreak would produce a general decrease in forest cover and that defoliated trees would show a strong reduction in radial growth and tracheid lumen diameter and, accordingly, an increase in wood density. Defoliated trees would also show lower $\delta^{13}\text{C}$ values of wood cellulose related to old needle loss and impairment of N resorption by new needles, leading to N-depleted, less water-use-efficient current-year needles driving the tree carbon balance. This would be accompanied with a stronger coupling between $\delta^{13}\text{C}$ and oxygen isotope composition ($\delta^{18}\text{O}$) reflecting the variable yearly contribution to photosynthesis of needles from different cohorts following the defoliation event. We also expected that defoliated pines would show a lower responsiveness to drought severity in terms of growth and wood density due to the impacts of PPM defoliation as compared with non-defoliated pines, whose tree-

ring width and density series would be more coupled to changes in soil water availability.

2 Materials and methods

2.1 Study sites

We selected two 50-year-old *P. nigra* plantations where PPM outbreaks and severe defoliations were observed from winter 2015–2016 to spring 2016 (Figure S1). These plantations are located in the Aragón region (north-eastern Spain), and they are named hereafter Huesca (42.557° N, 0.342° W, 875 m a.s.l., located near Senegüé village) and Teruel (40.190° N, 0.652° W, 1150 m a.s.l., located near Mora de Rubielos village) sites. The cover of the plantations ranges from 70% (Teruel) to 90% (Huesca) with a mean tree-to-tree distance of 4–6 m. The natural vegetation is dominated by oak species (*Quercus ilex* L., *Quercus faginea* Lam.) and junipers (*Juniperus communis* L., *Juniperus oxycedrus* L.) in both sites. Soils are basic, nutrient-poor and developed on flysch substrates in Huesca and on clays in Teruel. The Teruel site is situated in a region where intensive monitoring of PPM defoliations has been carried out since the 1970s (Montoya and Hernández, 1991; Gazol et al., 2019).

Since *Q. faginea* is naturally present in the vicinity of plantations at both sites, this winter-deciduous oak species with ring-porous wood was selected as control, non-defoliated species. Radial growth reduction in 2016 after the severe defoliation episode ranged from –92% (Huesca) to –99% (Teruel) compared to previous years (Castaño et al., 2020). Further details on site characteristics are given in Palacio et al. (2012) and Castaño et al. (2020).

These two sites were selected because of their contrasting climate conditions. Climate data (mean monthly maximum and minimum temperatures and total precipitation, period 1980–2016) for the Huesca and Teruel sites were obtained from the nearby Biescas (42.628° N, 0.325° W, 860 m a.s.l.) and Mora de Rubielos (40.253° N, 0.753° W, 1038 m a.s.l.) meteorological stations, respectively (Figure S2). These data show that the Huesca site is cooler and wetter (9.3° C mean annual temperature, 808 mm total annual precipitation) than the Teruel site (11.6° C mean annual temperature, 491 mm total annual precipitation), where the summer drought is more severe and lasts longer (Figure S2). To assess changes in drought severity which could affect growth responses, we downloaded weekly values of the Standardized Precipitation Evapotranspiration Index (SPEI) drought index at 1.1 km² resolution (Vicente-Serrano et al., 2017) from the Spanish SPEI database (<https://monitordesequia.csic.es>). Series for the common period 1980–2016 were obtained for the Huesca and Teruel sites at the following temporal resolutions: 1, 3, 6, 9, 12 and 24 months. Dry conditions occurred in 1994–1995 (particularly in Teruel), 2005 and 2012 (Figure S3).

2.2 Remote sensing information

We used remote-sensing data to assess how the PPM defoliation event impacted canopy greenness and tree cover. For the period 1990–2021, we calculated the Normalized Difference Vegetation Index

(NDVI), which is based on how healthy green vegetation differently reflects red and near-infrared radiation (Tucker, 1979), and the kernel NDVI (KNDVI), a non-linear version of the NDVI which is more accurate in detecting changes in leaf area index (Camps-Valls et al., 2021). We also considered the Normalized Difference Infrared Index (NDII; see Hunt and Rock, 1989) since it was found to detect severe defoliation due to PPM outbreaks (Sangüesa-Barreda et al., 2014). In the case of NDII, we analyzed 456 and 437 scenes (16-day averaged composites) taken at similar dates in Huesca and Teruel sites, respectively, during 2000–2022. In all cases we applied cloud masks using the CFMask algorithm and using a 40% cloud threshold in addition to radiometric and topographic corrections using the USGS GMTED2010 digital elevation model (Hantson and Chuvieco, 2011). Lastly, we harmonized Landsat ETM+ surface reflectance records to Landsat 8 OLI surface reflectance series (Roy et al., 2016). We considered 50-m buffer areas around each site to quantify the three vegetation indices. These calculations were carried out using the Google Earth Engine platform (<https://earthengine.google.com>, accessed on 28 September 2022).

2.3 Field sampling and tree selection

Tree selection was carried out in February 2016, following the conclusion of the outbreak, and tree sampling was conducted in the spring of the same year. In both study sites, a small percentage of non-defoliated pine trees (mean defoliation 0–3%, hereafter ND trees) coexisted with defoliated (mean defoliation 95–99%, hereafter D trees) neighboring pines (Figure S1). Therefore, we randomly selected pairs of defoliated ($n = 15$ trees) and non-defoliated ($n = 15$ trees) neighboring pine trees at each site within an area of ca. 2000 m² as in Castaño et al. (2020). Since susceptibility to PPM defoliation increases at stand edges (Règolini et al., 2014), trees were sampled inside the forest to avoid any edge effect (>10 m from the plantation edge). Crown defoliation was visually estimated by two observers and averaged for each sampled pine. We performed a paired sampling approach (e.g., each defoliated tree had its non-defoliated tree pair located within 10 m) to reduce confounding spatial effects. The sampled oak stands were located at 10–20 m from the pine plantations. In the case of oaks, 15 mature trees were also sampled.

We also measured the diameter at 1.3 m of sampled trees. It was 24.6 ± 3.3 cm (mean \pm SE) and 15.0 ± 1.6 cm in the Huesca and Teruel sites, respectively, with no significant differences between D and ND pine trees (t tests, $p > 0.05$). In the case of oaks, it was 15.7 ± 1.2 cm and 11.9 ± 0.4 cm in the Huesca and Teruel sites, respectively. The mean ages (at 1.3 m) of pines were 37 ± 2 years and 36 ± 2 years in Huesca and Teruel, respectively, whereas the mean ages of oaks were 40 ± 2 and 46 ± 3 years, respectively.

2.4 Tree-ring width data

Dendrochronological methods were used to quantify the radial growth of trees since 1980 (Fritts, 1976). Two increment wood cores from each tree were extracted at breast height (1.3 m) using 5-mm increment corer (Haglöf, Långsele, Sweden) to measure tree-ring

width. These cores were air-dried, glued onto wooden supports and then carefully sanded until tree-ring boundaries were clearly visible. A third core was extracted from 10 ND and 10 D pines in each site for densitometry analyses.

Tree rings were visually cross-dated, and their width (RW), earlywood (EWW) and latewood (LWW) widths were measured to the nearest 0.001 mm using a binocular microscope and a LINTAB measuring device (Rinntech, Heidelberg, Germany). Earlywood and latewood were visually distinguished by an abrupt transition along the radial file of tracheids from early to latewood from tracheids with wide lumen and thin walls to tracheids with narrow lumen and thick walls (Camarero et al., 2021). The visual cross-dating was checked using the COFECHA program, which calculates correlations between each individual series with the mean series of each group of trees (defoliated pines, non-defoliated pines and non-defoliated oaks) at each site (Holmes, 1983).

2.5 Inter-annual changes in wood density

To assess year-to-year changes in wood density, cores from 10 ND and 10 D pines from each site were used. First, thin (ca. 1.3-mm thick) wood samples were transversally cut using a Dendrocut table saw (Walesch Electronic GmbH, Zurich, Switzerland). Wooden laths were kept under constant temperature (20 °C) and humidity (40%) in the CETEMAS wood laboratory (Asturias, Spain) micro-densitometry laboratory, before being X-ray scanned in an Itrax Multiscanner (Cox Analytical Systems, Sweden). The samples were exposed to 30 kV, 30 mA for 25 ms in the radial direction (50- μ m step size) using a copper tube.

Wood density profiles were obtained for each sample using the Win-Dendro software (Regent Instruments, Québec, Canada). The measured ring-width series of radiographic images were visually cross-dated, and compared with chronologies developed using tree-ring width data. Minimum (MnD) and maximum (MxD) wood density values per tree-ring (in g cm^{-3}) were extracted from the radiographic images by calibrating the grey-scale intensities using a light calibration curve derived from a calibration step-wedge. A final check of the visual cross-dating based on tree-ring widths was carried out by using the COFECHA software as before. We focused on MnD and MxD because they do not depend on the definition of earlywood and latewood and MnD usually shows strong responses to spring drought in *P. nigra* and other conifers (Camarero et al., 2014; Camarero and Hevia, 2020). MnD and MxD corresponded to the lowest and highest density values along the density profile of a tree-ring, respectively.

2.6 Processing tree-ring width and wood density data

To reflect growth changes through time, tree-ring width series were transformed to basal area increment (BAI) series assuming circular growth of stems. Then the ring-width, MnD and MxD series were subjected to detrending and standardization to remove long-term trends and to retain the year-to-year variability (Fritts, 1976). These procedures allowed the calculation of the mean, detrended

series or chronologies for each variable and type of trees (ND and D pines, ND oaks), which were further correlated with monthly climate variables (mean maximum and minimum temperatures, precipitation) and weekly SPEI data considering the period 1980–2016. First, we applied a power (Box-Cox) transformation to the individual density series to reduce heteroscedasticity. Second, a smoothing spline with a 50% frequency response at a wavelength of 20 years was fitted to individual series. Then, ring-width (RW, EWW, LWW) and density (MnD and MxD) indices were obtained by dividing or subtracting, respectively, the fitted values from the observed values. The resulting indices were subjected to autoregressive modeling to remove first-order autocorrelation. Then, the individual series were averaged by tree type and species (ND and D pines, ND oaks) on a yearly basis using a bi-weight robust mean to produce mean series of pre-whitened indices or residual chronologies (Fritts, 1976). These procedures were performed using the ARSTAN v 4.4 software (Cook and Krusic, 2007).

The ring-width and density (EWW, LWW, MnD, MxD) indexed series calculated at individual levels for each group (ND and D pines) were correlated with monthly climate variables (mean maximum and minimum temperatures and total precipitation) from previous October to current September and also considering the growing season (April to July).

Outbreak defoliation signals in tree-ring width data are usually analyzed by comparing standardized tree-ring width series from host (in our case *P. nigra*) and non-host tree species (in our case the oak *Q. faginea*) (Swetnam et al., 1985). A similar procedure was followed by Camarero et al. (2022a) to reconstruct PPM outbreaks near the Teruel study site. Here we followed a similar approach by comparing (i) individual and mean series of ring-width indices of host and non-host tree species in each site, and (ii) correlations between individual and mean series of ring-width and density (MnD, MxD) and the SPEI.

2.7 Wood anatomy

In an additional sampling campaign in 2018, we took cores of D pines in the Teruel and Huesca sites. Thin transversal wood sections (10–15 μ m thick) were obtained using a sledge core microtome (Gärtner and Nievergelt, 2010). This was done in four cores from four D pines sampled in both study sites and showing a clear narrow ring in 2016 (i.e. associated to the PPM outbreak). Sections included the 2016 ring and two 2-year reference periods, previous (i.e., 2014–2015) and subsequent (i.e., 2017–2018) to the PPM outbreak. Sections were mounted on glass slides, stained with safranin (0.5% in distilled water) and fixed with Eukitt[®]. Images of sections were first taken at 40–100 \times magnification with a digital camera mounted on a light microscope (Olympus BH2, Tokyo, Japan) and then stitched with the Image Composite Editor software (Interactive Visual Media, Microsoft 2023, Redmond, USA).

Images were analyzed for xylem measurement using the software ImageJ v.1.40 (Schneider et al., 2012). In particular, lumen radial diameter (LD) and the double cell wall thickness (CWT) were measured for each tracheid along five radial rows for the 2014–2018 period using the ‘plot profile’ function. This function allowed discriminating between tracheid walls and lumen according to the

variation of pixels' grey intensity along a line passing through a tracheid radial file. To compare patterns of cell dimensions between and within rings, the number of cells was standardized to 20 by using the tracheidogram method (Vaganov et al., 2006) with the 'tgram' package (DeSoto et al., 2011) in the R version 3.6.0 environment (R Core Team, 2022).

Trends and trend changes (breakpoints) in LD and CWT time series were analyzed through an additive decomposition model using the 'greenbrown' package (Forkel et al., 2013) in R version 4.2.1 environment (R Core Team, 2022). In detail, we used the Seasonal Trend Model method, based on the classical additive decomposition model (Verbesselt et al., 2012), where linear and harmonic terms are fitted to the original time series using ordinary least squares regression. The significance of the trend was estimated using *t* tests. The breakpoint detection algorithm searches for structural changes in the regression and estimates their position by minimizing the residual sum of squares (Forkel et al., 2013). When a breakpoint is detected, the trend is divided into two segments whose slopes may or may not be significant. Lastly, we used *t* tests and ANOVAs to check if there were significant ($p < 0.05$) differences in both tracheid traits (LD, CWT) between the outbreak year (2016) and the previous (2014–2015) and subsequent 2-year periods (2017–2018).

2.8 Raman spectroscopy

We used confocal Raman micro-spectroscopy to investigate the chemical composition (lignification) of tracheid cell-walls (Gierlinger et al., 2012; Gierlinger, 2014; Agarwal, 2019). Raman imaging allows the quantification of the chemical composition of cell walls without altering their structure. As in the wood anatomy data, we compared the ring formed during the defoliation year (2016) vs. the previous (2015) and following (2017) rings. We selected for these analyses five D pines from Huesca; the lack of material prevented the application of this analysis in trees from Teruel. As in the case of wood anatomy, thin wood cross sections were obtained although they were not stained. We mounted each section on microscope slides. After gently pressing the cover glass to remove the excess of denatured water, samples were semi-permanently fixed.

A Raman microscope (LabRAM HR, Horiba Jovin Yvon Scientific, Kyoto, Japan) equipped with laser excitation energies of 2.33 eV (532 nm, Ar/Kr laser, Coherent) was used. A 100× objective with a laser spot of about 1 mm was employed. The laser power was around 1 mW and the spectral resolution was 1 cm^{-1} . The WITec Project Plus software was used for data analysis (WITec, Ulm, Germany). Raman imaging was performed on earlywood and latewood zones focusing on the cell corners of tracheid cell-walls because stress factors such as drought or insect defoliation cause reduced lignification of the middle lamella and outer secondary cell walls in these areas where lignification processes start (Donaldson, 2002). We measured areas of about 2000–3000 μm^2 . For each tree ring, 30 images were captured and analyzed (15 in earlywood tracheids and 15 in latewood tracheids) to obtain average values of lignin/carbohydrate (particularly cellulose) ratios, which are based on the Raman intensity of the

lignin and carbohydrate bands and reflect the degree of lignification (Hänninen et al., 2011).

2.9 C and O isotopes in wood cellulose

We selected eight D and nine ND pine individuals in each site. We investigated the period 2015–2018 to include the 2016 defoliation event in both sites. Annual rings were separated under the microscope using scalpels. Wood samples were milled and homogenized using a ball mixer mill (Retsch MM301, Haan, Germany). Then, wood α -cellulose was extracted for C and O isotope analyses (Loader et al., 1997; Ferrio and Voltas, 2005; Shestakova et al., 2017). Sodium hydroxide was used to obtain α -cellulose which was homogenized to a fine powder with a ball mixer mill (Retsch MM301, Haan, Germany). An aliquot of 0.3–0.4 mg of dry α -cellulose was weighed on a balance (Mettler Toledo AX205, OH, USA) and placed into tin and silver capsules for $\delta^{13}\text{C}$ and $\delta^{18}\text{O}$ analyses, respectively. In Teruel, we could obtain enough wood material only for two D pines and 3 ND pines because of the very narrow 2016 ring. This did not allow extracting enough cellulose for $\delta^{13}\text{C}$ and $\delta^{18}\text{O}$ analyses which were not done. For $\delta^{13}\text{C}$, capsules were combusted to CO_2 using a Flash EA-1112 elemental analyzer interfaced with a Finnigan MAT Delta C isotope ratio mass spectrometer (Thermo Fisher Scientific Inc., MA, USA). For $\delta^{18}\text{O}$, capsules were combusted using a Carlo Erba 1108 elemental analyzer (Carlo Erba Instruments Ltd, Milan, Italy) interfaced with a Finnigan Deltaplus XP isotope ratio mass spectrometer (Thermo Fisher Scientific Inc., Bremen, Germany). Isotope analyses were carried out at the Stable Isotope Facility of the University of California (Davis, USA). Stable isotope ratios were expressed as per mil deviations using the δ notation relative to Vienna Pee Dee Belemnite (VPDB) for C isotopes and the Vienna Standard Mean Ocean Water standard for O isotopes. The accuracy of the analyses (standard deviation of working standards) was 0.06‰ ($\delta^{13}\text{C}$) and 0.25‰ ($\delta^{18}\text{O}$).

2.10 Statistical analyses

Comparisons of variables (NDII, tree-ring width, BAI, EWW, LWW, LD, CWT, MnD, MxD, lignin/carbohydrate ratio, correlations between ring-width or density indices and climate variables) between sites or between ND and D pine trees were performed using *t* tests. Comparisons between slopes of $\delta^{18}\text{O}$ vs. $\delta^{13}\text{C}$ linear regression were done using an ANCOVA. We used Wilcoxon rank-sum tests to check if the changes through time in growth (BAI) differed between defoliation classes at each study site.

3 Results

3.1 Remote sensing data

The annual NDVI series showed a clear drop in the 2016 year following the PPM outbreak (Figure S4). The relative NDVI

(KNDVI) drop in 2016 was -10.5% (-20.5%) and -10.8% (-24.6%) in Huesca and Teruel, respectively. We also found a notable KNDVI drop of -17.3% in 1993 for Huesca. Regarding the NDII, the annual relative reductions measured in 2016 were -47.3% and -55.6% in Huesca and Teruel, respectively (Figure 1). The NDII showed minimum values from late March to late April 2016. The NDII was significantly higher (paired- $t = 28.5$, $p < 0.001$) in Huesca (mean \pm SD, 0.22 ± 0.07) than in Teruel (0.09 ± 0.06). All vegetation indices (NDVI, KNDVI, NDII) indicated that the recovery time was faster (about one year shorter) in Huesca than in Teruel.

3.2 Changes in radial growth linked to PPM defoliation

The PPM defoliation markedly reduced radial growth in 2016 (Table 1; Figures 2, 3, S5). The mean reduction in BAI was -93.3% and -99.3% in Huesca and Teruel, respectively (Figure 3). Similar reductions in ring-width were observed (Figure S5). The BAI (mean \pm SE) was higher in D pines ($4.51 \pm 0.45 \text{ cm}^2$) than in ND pines ($3.41 \pm 0.39 \text{ cm}^2$) from Huesca, but differences were only marginally significant ($t = 1.83$, $p = 0.07$). In the drier Teruel site, growth rates were again

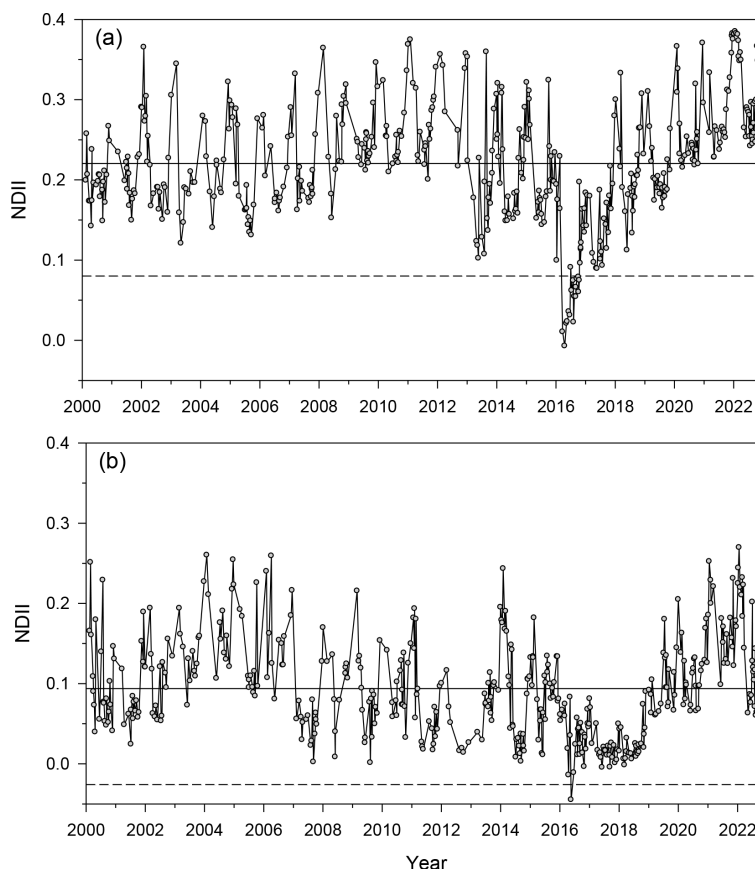


FIGURE 1 Values of the NDII vegetation index calculated in (A) Huesca and (B) Teruel sites during 2000–2022. The 2016 NDII drop corresponds to a severe PPM defoliation. Continuous and dashed horizontal lines indicate the mean and the mean $- 1.96$ SD (95% confidence interval) values, respectively.

TABLE 1 Radial growth and wood density statistics obtained in defoliated (D) pines and non-defoliated (ND) pines (*P. nigra*) and oaks (*Q. faginea*) from Huesca and Teruel sites.

| Site | Species | Type | RW (mm) | EW (mm) | LWW (mm) | MnD (g cm^{-3}) | MxD (g cm^{-3}) |
|--------|-------------------|------|-------------------------|-------------------------|-------------------------|----------------------------|----------------------------|
| Huesca | <i>P. nigra</i> | D | $1.92 \pm 0.14\text{b}$ | $1.52 \pm 0.10\text{b}$ | $0.51 \pm 0.03\text{a}$ | $0.42 \pm 0.01\text{a}$ | $1.01 \pm 0.01\text{a}$ |
| | | ND | $1.80 \pm 0.11\text{b}$ | $1.10 \pm 0.08\text{a}$ | $0.58 \pm 0.05\text{a}$ | $0.43 \pm 0.01\text{a}$ | $0.97 \pm 0.01\text{a}$ |
| | <i>Q. faginea</i> | ND | $1.39 \pm 0.04\text{a}$ | – | – | – | – |
| Teruel | <i>P. nigra</i> | D | $1.62 \pm 0.18\text{b}$ | $1.24 \pm 0.13\text{a}$ | $0.40 \pm 0.04\text{a}$ | $0.44 \pm 0.01\text{a}$ | $0.91 \pm 0.02\text{a}$ |
| | | ND | $1.51 \pm 0.17\text{b}$ | $1.16 \pm 0.13\text{a}$ | $0.35 \pm 0.03\text{a}$ | $0.45 \pm 0.01\text{a}$ | $0.90 \pm 0.02\text{a}$ |
| | <i>Q. faginea</i> | ND | $0.66 \pm 0.04\text{a}$ | – | – | – | – |

RW, tree-ring width; EW, earlywood width; LWW, latewood width; MnD, minimum wood density; MxD, maximum wood density. Values are means \pm SE calculated for the common period 1980–2016 excepting density values in Teruel (period 1980–2015). Different letters indicate significantly ($p < 0.05$) different values between groups of trees within the same site according to t tests.

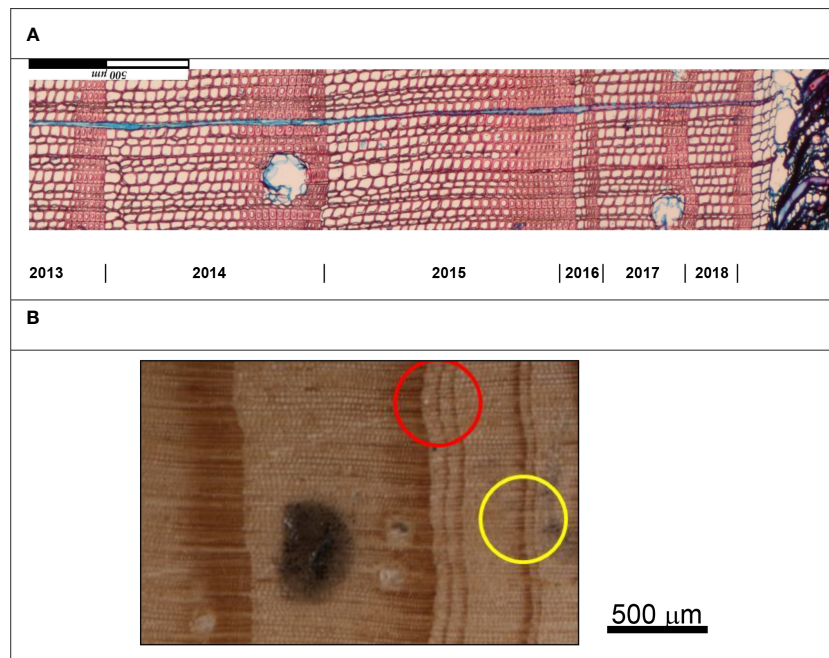


FIGURE 2 (A) View of several rings in a *Pinus nigra* tree severely defoliated by PPM in the Teruel site showing the narrow 2016 ring corresponding to the 2015–2016 PPM outbreak. The bar indicates 0.5 mm. (B) Difficult to distinguish narrow rings due to PPM defoliation (red circle) or to severe drought (yellow circle) in a core from a defoliated *P. nigra* tree growing in a natural stand located at 1200 m a.s.l. near the Teruel site. The black area indicates the ring formed in 1990. Image (B) is based on Camarero et al. (2022a).

higher in D pines ($3.14 \pm 0.30 \text{ cm}^2$), but not statistically different from those measured in ND pines ($2.72 \pm 0.25 \text{ cm}^2$). In both sites, the RW of ND or D pines was significantly higher than the oaks' RW ($t = 4.45, p < 0.001$; Table 1). Oak growth rates were always lower than those of

pines (Figure S6). In Huesca, D pines grew more than ND pines from 1981 to 1992, from 1995 to 1998 and also from 2001 to 2015 ($p < 0.05$; Wilcoxon rank-sum tests). In Teruel, this occurred from 1982 to 1987, from 1995 to 2005, and in 2009 and 2010. Regarding other tree-ring

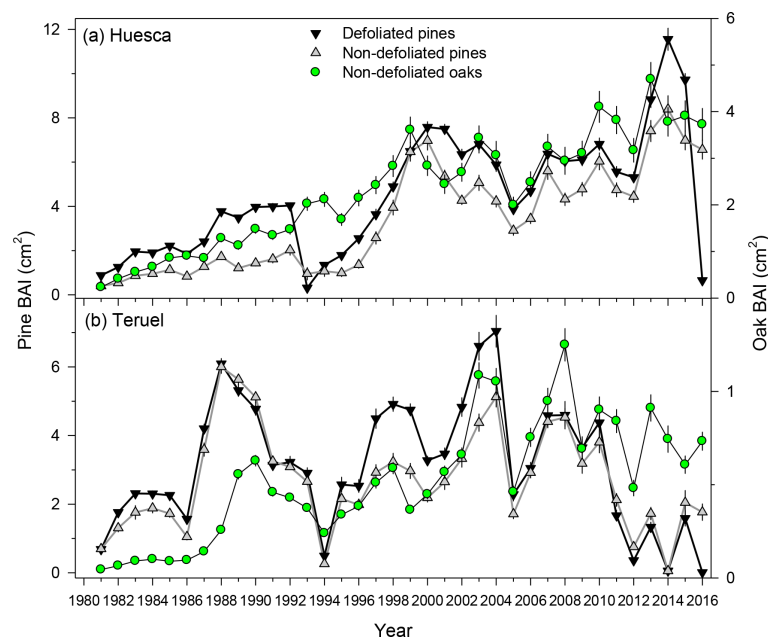


FIGURE 3 Growth variability and trends (BAI, basal area increment) in defoliated and non-defoliated pines and non-defoliated oak trees from (A) Huesca and (B) Teruel sites. Values are means \pm SE. Note the different BAI scales.

variables, we only found significantly higher EWW in D than in ND pines from Huesca (Table 1).

In each site, growth reductions of the two tree species were usually associated with dry years such as 1994–1995, 2005 and 2012 (Figures 3, S6), excepting the 1993 narrow ring in Huesca which likely corresponds to a previous PPM defoliation (*pers. observ.*). In both sites, the three BAI series were significantly ($p < 0.05$) and positively correlated. In Huesca, the highest correlation corresponded to the comparison between ND pines and oak BAI series ($r = 0.90$), whereas in Teruel it was for the comparison between ND and D pines ($r = 0.91$).

No significant differences were found between ND and D pines when comparing EWW, LWW (Figure S7), MnD or MxD series (Figure S8), except that D pines showed higher EWW values than ND pines in Huesca (Table 1).

3.3 Changes in wood anatomy associated with PPM defoliation

In both sites a significant reduction in LD was detected in the 2016 ring (relative reductions in maximum LD were -32.4% and

-37.5%, respectively, for Huesca and Teruel). These reductions caused marked breakpoints (Figure 4). Significant differences were detected in the average LD in 2016 compared to the prior (2014–2015) and subsequent (2017–2018) periods (Huesca, $F = 4.82$, $p = 0.029$; Teruel, $F = 5.69$, $p = 0.013$). In Teruel, LD in 2016 was smaller than in the previous 2-year period ($t = -3.35$, $p = 0.010$), but not with respect to the subsequent 2-year period ($t = 1.91$, $p = 0.165$), whereas the pre- and post-outbreak periods did not significantly differ ($t = -1.80$, $p = 0.200$). Similarly, in Huesca, LD in 2016 was smaller than in the previous year ($t = -3.05$, $p = 0.024$), but not similar to the subsequent ($t = 2.44$, $p = 0.073$) 2-year period, whereas the pre- and post-outbreak periods did not significantly differ ($t = -0.74$, $p = 0.738$). The CWT values differed between 2016 and the preceding or following periods only in Huesca (Figure S9).

3.4 Raman spectroscopy

In the five defoliated pines analyzed, the lignin/carbohydrate ratios were significantly ($p < 0.05$) lower in the defoliation year (2016) than in the previous (2015) and following (2017) years both in the earlywood and in the latewood cell walls (Table 2). Ratios were

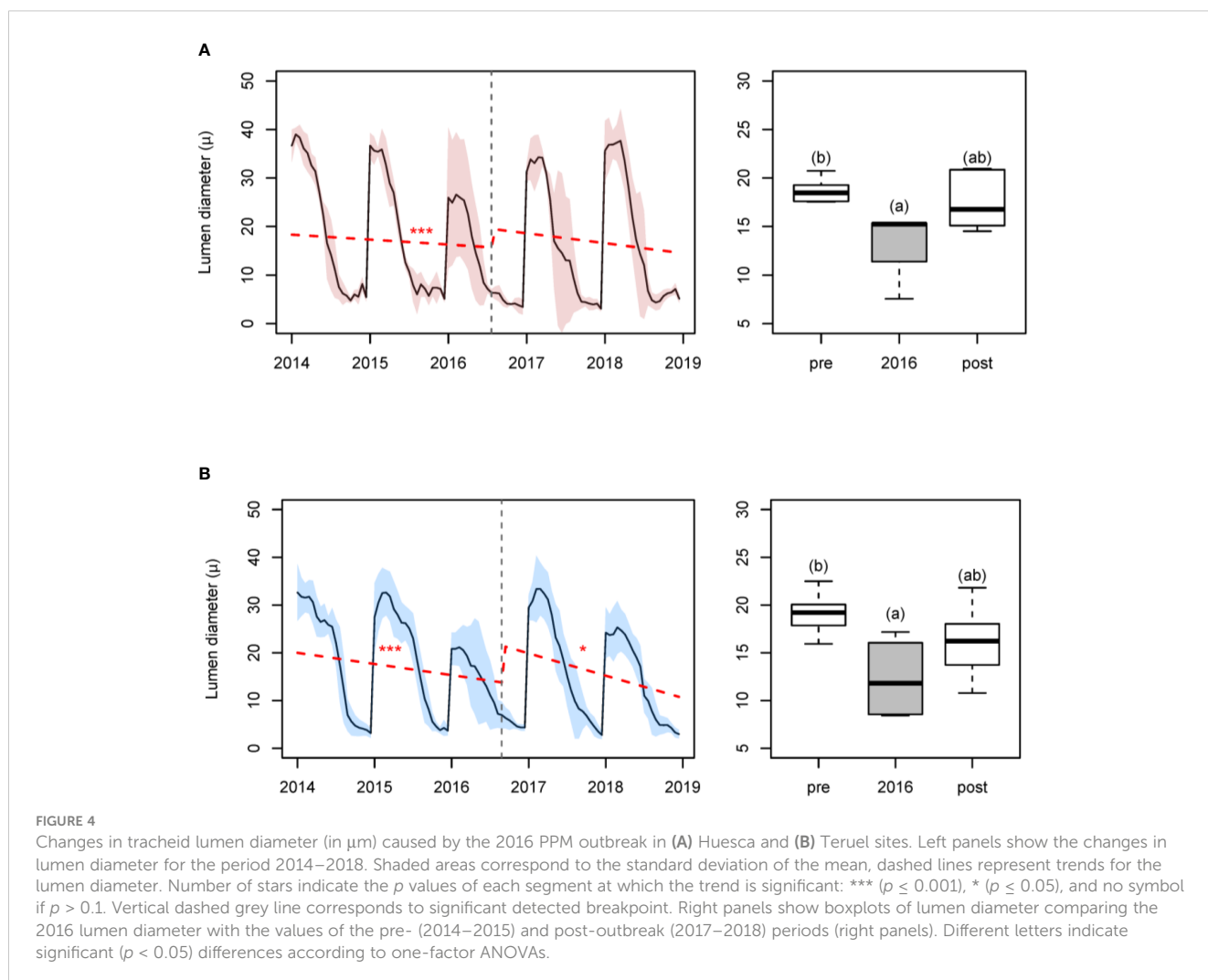


TABLE 2 Mean values of the lignin/carbohydrate ratio obtained through Raman spectroscopy in five defoliated pines (*P. nigra*) from the Huesca site.

| Tree | Wood type | Years | | |
|------|-----------|--------------|--------------|--------------|
| | | 2015 | 2016 | 2017 |
| 1 | EW | 2.49 ± 0.09b | 2.00 ± 0.01a | 2.38 ± 0.16b |
| | LW | 2.67 ± 0.04b | 2.27 ± 0.01a | 3.43 ± 0.15c |
| 2 | EW | 2.56 ± 0.06b | 1.84 ± 0.05a | 2.51 ± 0.10b |
| | LW | 2.73 ± 0.04b | 2.05 ± 0.03a | 3.49 ± 0.06c |
| 3 | EW | 2.73 ± 0.07b | 2.08 ± 0.04a | 2.44 ± 0.07b |
| | LW | 2.99 ± 0.06b | 2.35 ± 0.06a | 3.03 ± 0.18b |
| 4 | EW | 2.47 ± 0.10b | 1.97 ± 0.04a | 2.39 ± 0.03b |
| | LW | 2.70 ± 0.05b | 2.41 ± 0.04a | 2.75 ± 0.06b |
| 5 | EW | 2.58 ± 0.07b | 1.99 ± 0.05a | 2.46 ± 0.08b |
| | LW | 2.79 ± 0.07b | 2.26 ± 0.06a | 3.07 ± 0.11c |

Values (means ± SE) are reported for cell walls of earlywood (EW) and latewood (LW) tracheids considering the defoliation year (2016) and the previous and following years. Different letters indicate significantly ($p < 0.05$) different values between years and within the same tree according to t tests.

lower in the earlywood (2.32 ± 0.08) than in the latewood (2.74 ± 0.13). The highest ratios for latewood were found in the 2017 ring.

3.5 C and O isotopes in wood cellulose

In Huesca, $\delta^{13}\text{C}$ values were significantly lower ($t = -3.17$, $p = 0.007$) in D pines (mean ± SE, -25.61 ± 0.20 ‰) than in ND pines (-24.90 ± 0.11 ‰), but no significant differences were observed regarding $\delta^{18}\text{O}$ (mean value = 33.60 ‰; Figure 5). There was a clear drop in $\delta^{13}\text{C}$ values from 2015 to 2016 in defoliated pines (-0.79 ± 0.09 ‰) which was stronger ($t = -22.5$, $p < 0.001$) than in non-defoliated pines (-0.27 ± 0.02 ‰). In this site, the positive

relationship between $\delta^{13}\text{C}$ and $\delta^{18}\text{O}$ values was stronger in D than in ND pines ($r = 0.80$ and $r = 0.70$, respectively), and the slope of this relationship was also significantly higher in D pines ($F = 15.30$, $p = 0.002$; 0.54 ± 0.12 vs. 0.30 ± 0.10 in D vs. ND trees, respectively).

3.6 Responses of ring-width and minimum wood density to climate variables and drought

Overall, pine growth was enhanced by cool-wet conditions in spring and summer, particularly in the drier Teruel site (Figure S10). In this site, dry spring conditions were strongly associated with high MnD values.

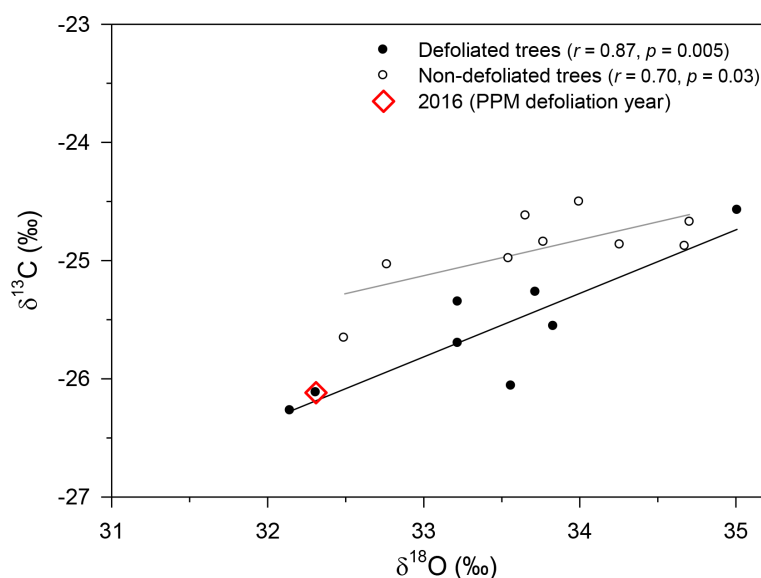


FIGURE 5

Relationships between $\delta^{13}\text{C}$ and $\delta^{18}\text{O}$ values from defoliated and non-defoliated pine trees in Huesca site. Lines indicate significant ($p < 0.05$) linear relationships.

When comparing the climate-growth/density correlations at the individual level between ND and D pines, we found two different responses. In Huesca, the LWV of D pines responded more ($t = 3.19$, $p = 0.015$) to July rainfall ($r = 0.26 \pm 0.05$) than in the case of ND pines ($r = 0.14 \pm 0.03$). In Teruel, the negative relationship between MnD and April rainfall was stronger ($t = -7.16$, $p < 0.001$), in absolute terms, in ND ($r = -0.39 \pm 0.05$) than in D pines ($r = 0.11 \pm 0.04$). In this site, the MnD of ND trees also decreased in response to high March precipitation (Figure S10).

Growth series of pines from Huesca (6-month SPEI, SPEI6) responded to longer droughts than those of pines from Teruel (3-month SPEI, SPEI3; Figure 6). In Huesca, the growth of ND trees responded more to SPEI6 than growth of D trees with correlations peaking in August. In Teruel, the MnD of ND pines responded more negatively to SPEI3 than in the case of D pines with correlations peaking in absolute terms in May (Figure 6).

4 Discussion

The framework applied in this case study to evaluate the impacts of PPM on *P. nigra* plantations allowed us to differentiate the responses of coexisting host (pines) and non-host (oaks) species to insect defoliation and droughts such as those occurring in 2005 and 2012. Furthermore, we extended the classical approach of comparing host vs. non-host tree species by including additional variables which provided complementary information to pinpoint the insect outbreaks. Altogether, we advocate for a more widespread use of multi-proxy approaches to detect the impacts of severe insect defoliations on tree growth and functioning.

First, remote-sensing vegetation indices (NDII, KNDVI) showed strong reductions in tree cover as observed in other studies where insects partially (Sangüesa-Barreda et al., 2014) or completely defoliated stands (Camarero et al., 2022b). In fact, the

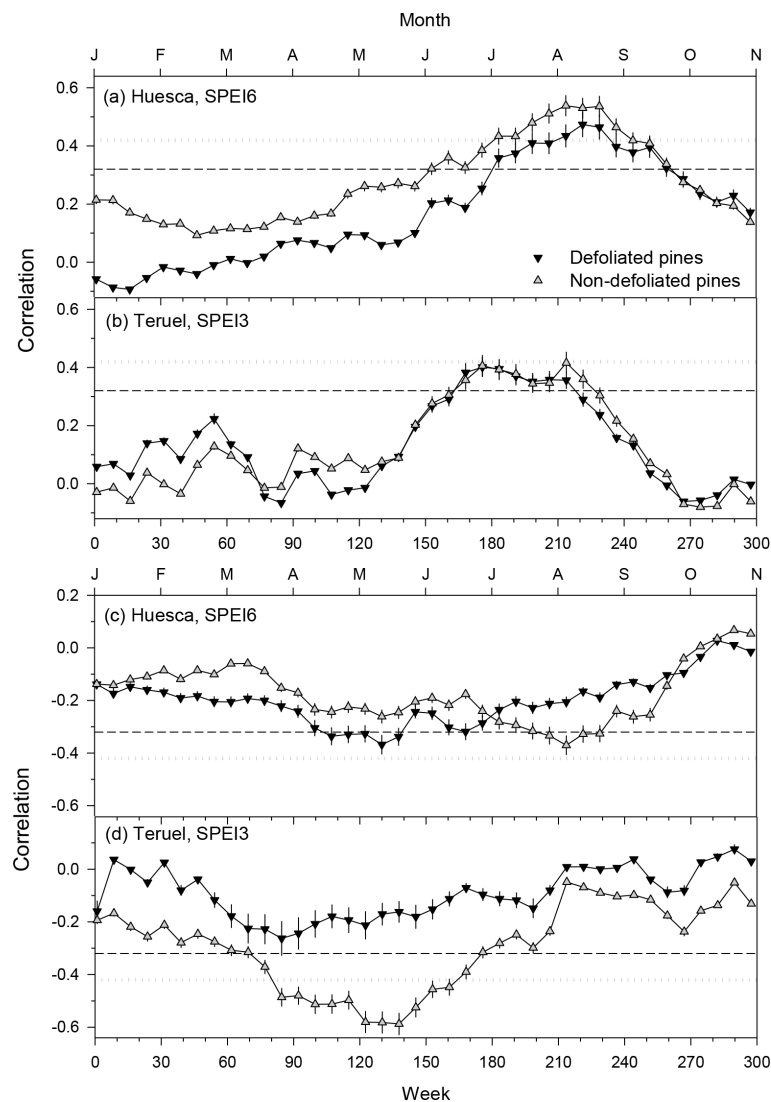


FIGURE 6

Relationships (Pearson correlations) between weekly values of the SPEI drought index and series of ring-width (plots A, B) or minimum wood density (plots C, D) indices of defoliated and non-defoliated pines in the Huesca and Teruel sites. In each plot, the selected SPEI temporal resolution is indicated (e.g., SPEI6 corresponds to a 6-month resolution). Horizontal dashed and dotted lines indicate 0.05 and 0.01 significance levels, respectively.

NDII was already used as an efficient index to detect PPM defoliation with very low values corresponding to strong defoliation events (Sanguesa-Barreda et al., 2014). Our findings concur with these analyses.

Second, defoliated pines showed a strong reduction in growth, as expected and in agreement with previous meta-analyses (Jactel et al., 2012), but also in lumen diameter and, therefore, potential hydraulic conductivity. It has been found that severe PPM defoliation (50–60%) caused a reduction in lumen area of earlywood and latewood tracheids in *Pinus brutia* one year after the defoliation started (Güney, 2019). This finding also concurs with our results and indicates that rebuilding new foliage and forming new xylem cells in spring may incur a cost in terms of the radial enlargement of tracheids and their final lumen area, which influences how trees access and use water to provide enough turgor to cambium cells (Von Wilpert, 1991).

Third, defoliated pines presented lower cellulose $\delta^{13}\text{C}$ values, as hypothesized, and a stronger coupling between $\delta^{13}\text{C}$ and $\delta^{18}\text{O}$ values than their non-defoliated counterparts in the wet site. The first result indicates that the loss of old needles in these trees translated into a lower intrinsic water-use efficiency compared to the more efficient non-defoliated pines. Herbivory in the winter season may strongly impair nitrogen mobilization from old needles to new needles during growth resumption (Proe et al., 2000), thereby compromising photosynthetic capacity (Wyka et al., 2016) more than stomatal conductance. In fact, whole leaf conductance to water vapor has been shown to be consistently highest in the youngest, and lowest in the oldest, needle cohort of the phylogenetically close *P. sylvestris* (Wyka et al., 2016). In this regard, a stronger coupling of C and O isotopes (Scheidtger et al., 2000; Roden and Farquhar, 2012; Voltas et al., 2013; Shestakova et al., 2017) in defoliated pines suggests a broader range of stomatal responses scaling with rates of photosynthesis (Warren, 2006), which may be related to a varying net contribution of needles from different cohorts to the total tree carbon budget before, during and following the defoliation event. Despite the impacts of the severe PPM defoliation on radial growth, lumen diameter and C-O wood isotopes, the heavily defoliated pines recovered one year after the outbreak and showed normal growth and wood-anatomical values. In a long-term experiment with induced PPM severe defoliation near the Teruel site, radial growth was impaired but trees accumulated and stored non-structural carbohydrates showing no source limitation but a reduced C-sink demand and a decrease in C allocation to growth (Palacio et al., 2012). Therefore, defoliated trees did not seem to present signs of carbon pools exhaustion. Further research could investigate if C depletion occurs in other organs such as roots since severe PPM defoliations can have cascading effects on root–fungi interactions and reduce the biomass of ectomycorrhizal fungi in soils below defoliated pines as was observed in the dry Teruel site (Castaño et al., 2020).

Fourth, growth of non-defoliated trees from the wet Huesca site responded more to mid-term summer droughts than that of defoliated trees, whereas in the dry Teruel site non-defoliated pines showed a higher minimum wood density responsiveness to

short spring droughts than defoliated trees. These two results suggest a higher growth dependence on soil water availability of less defoliated trees prior to the insect outbreak. However, in the wet site latewood production of defoliated trees depended more on summer rainfall than in non-defoliated trees. In another study on a gypsy moth outbreak, pre-outbreak differences in wood density and responses to climate (also with a higher dependence on precipitation in defoliated trees) were also observed in coexisting trees showing different susceptibility to insect defoliation (Camarero et al., 2018). It should be further investigated in other insect-tree species and along wide climatic gradients if there are other predisposing factors making conspecific trees more or less prone to insect defoliation. From a practical point of view, the tree-ring signal of PPM outbreaks seem to be more evident in the wet (Huesca) than in the dry (Teruel) site where drought also leads to the formation of narrow rings and dense wood (Camarero et al., 2022a).

Our findings suggest that PPM defoliation reduced the lignin concentration of tracheid cell walls, which probably indicated a lower or abnormal lignification as has also been observed in drought-stressed trees (Donaldson, 2002). Using Raman spectroscopy, it was found that the lignin content of fiber cell walls increased during outbreak years in the boreal shrub *Salix glauca*, while the content of carbohydrates decreased, i.e. there was an increase in the lignin/carbohydrate ratio (Prendin et al., 2021). This coincided with a sharp reduction in ring width and also in the transversal area of vessels (Prendin et al., 2020). This was interpreted as a decrease in C availability due to the insect defoliation which caused the formation of thinner and lignin-rich fiber cell walls maximizing wood mechanical stiffness. The different results of those studies compared with ours may depend on the fact that we examined a winter-feeding insect affecting conifers, whereas Prendin et al. (2020; 2021) analyzed spring-feeding insects defoliating deciduous hardwood species. Finally, the presented multi-proxy framework could be also used for detecting the impacts of other disturbances (e.g., wildfire) on tree growth and functioning by separating the influence of different stress factors.

We conclude that: (i) the patterns of radial growth and responses to climate alone may not be good indicators for reconstructing past insect defoliation events and outbreaks, and (ii) other wood variables or techniques (lumen area, minimum wood density, C and O isotopes, Raman spectroscopy) are more reliable indicators or tools for assessing the impacts of insect defoliation on tree functioning. In this study case involving PPM and *P. nigra*, defoliated pines showed lower growth, lumen diameter, $\delta^{13}\text{C}$ and responsiveness to climate than non-defoliated trees. Multi-proxy tree-ring analysis has the potential to improve our ability to reconstruct insect outbreaks using dendrochronology.

Data availability statement

The raw data supporting the conclusions of this article will be made available by the authors, without undue reservation.

Author contributions

JC, MC, and AR contributed to conception and design of the study. AR, AG, MP, AH and JV organized the database. JC and AR performed the statistical analysis. JC wrote the first draft of the manuscript. JV, AG, AR, MC, AH, and MP wrote sections of the manuscript. All authors contributed to manuscript revision, read, and approved the submitted version.

Funding

This research was funded by a Spanish Ministry of Science and Innovation project (TED2021-129770B-C21). AH was supported by “Action 7: Grants for the temporary incorporation of postdoctoral research staff, from the Operational Plan for Research Support of the University of Jaén (POAI-UJA)”, “Project LITHOFOR, RTI2018-095345-B-C21, Spanish Ministry of Science, Innovation and Universities, R&D Program Oriented to the Challenges of Society, 2018 Call”.

Acknowledgments

We thank Raúl Sánchez Salguero for his help in the field and Elvira Aylón Marquina for technical assistance with Raman

spectroscopy at Instituto de Carboquímica (ICB, CSIC) laboratories (Zaragoza, Spain).

Conflict of interest

The authors declare that the research was conducted in the absence of any commercial or financial relationships that could be construed as a potential conflict of interest.

Publisher's note

All claims expressed in this article are solely those of the authors and do not necessarily represent those of their affiliated organizations, or those of the publisher, the editors and the reviewers. Any product that may be evaluated in this article, or claim that may be made by its manufacturer, is not guaranteed or endorsed by the publisher.

Supplementary material

The Supplementary Material for this article can be found online at: <https://www.frontiersin.org/articles/10.3389/fevo.2023.1192036/full#supplementary-material>

References

- Agarwal, U. P. (2019). Analysis of cellulose and lignocellulose materials by raman spectroscopy: a review of the current status. *Molecules* 24, 1659. doi: 10.3390/molecules24091659
- Ayres, M. P., and Lombardero, M. J. (2000). Assessing the consequences of global change for forest disturbance from herbivores and pathogens. *Sci. Tot. Env.* 262, 263–286. doi: 10.1016/S0048-9697(00)00528-3
- Azcárate, F. M., Seoane, J., and Silvestre, M. (2023). Factors affecting pine processionary moth (*Thaumetopoea pityocampa*) incidence in Mediterranean pine stands: A multiscale approach. *For. Ecol. Manage.* 529, 120728. doi: 10.1016/j.foreco.2022.120728
- Battisti, A., Avci, M., Avtzis, D. N., Jamaa, M. L. B., Berardi, L., Berretima, W., et al. (2015). “Natural history of the processionary moths (*Thaumetopoea* spp.): new insights in relation to climate change,” in *Processionary Moths and Climate Change: An Update*. Ed. A. Roques (Dordrecht: Springer), 15–79. doi: 10.1007/978-94-017-9340-7_2
- Battisti, A., Stastny, M., Netherer, S., Robinet, C., Schopf, A., Roques, A., et al. (2005). Expansion of geographic range in the pine processionary moth caused by increased winter temperatures. *Ecol. Appl.* 15, 2084–2096. doi: 10.1890/04-1903
- Camarero, J. J., Álvarez-Taboada, F., Hevia, A., and Castedo-Dorado, F. (2018). Radial growth and wood density reflect the impacts and susceptibility to defoliation by gypsy moth and climate in radiata pine. *Front. Plant Sci.* 31. doi: 10.3389/fpls.2018.01582
- Camarero, J. J., Collado, E., Martínez-de-Aragón, J., De-Miguel, S., Büntgen, U., Martínez-Peña, F., et al. (2021). Associations between climate and earlywood and latewood width in boreal and Mediterranean Scots pine forests. *Trees Struct. Funct.* 35, 155–169. doi: 10.1007/s00468-020-02028-0
- Camarero, J. J., Gazol, A., Tardif, J. C., and Conciatori, F. (2015). Attributing forest responses to global-change drivers: limited evidence of a CO₂-fertilization effect in Iberian pine growth. *J. Biogeogr.* 42, 2220–2233. doi: 10.1111/jbi.12590
- Camarero, J. J., and Hevia, A. (2020). Links between climate, drought and minimum wood density in conifers. *IAWA J.* 41, 236–255. doi: 10.1163/22941932-bja10005
- Camarero, J. J., Rozas, V., and Olano, J. M. (2014). Minimum wood density of *JuniPerus thurifera* is a robust proxy of spring water availability in a continental Mediterranean climate. *J. Biogeogr.* 41, 1105–1114. doi: 10.1111/jbi.12271
- Camarero, J. J., Shestakova, T. A., and Pizarro, M. (2022b). Threshold responses of canopy cover and tree growth to drought and Siberian silk moth outbreak in southern taiga spruce forests. *Forests* 13, 768. doi: 10.3390/f13050768
- Camarero, J. J., Tardif, J., Gazol, A., and Conciatori, F. (2022a). Pine processionary moth outbreaks cause longer growth legacies than drought and are linked to the North Atlantic Oscillation. *Sci. Tot. Env.* 819, 153041. doi: 10.1016/j.scitotenv.2022.153041
- Camps-Valls, G., Campos-Taberner, M., Moreno-Martinez, A., Walther, S., Duveiller, G., Cescatti, A., et al. (2021). A unified vegetation index for quantifying the terrestrial biosphere. *Sci. Adv.* 7, 9. doi: 10.1126/sciadv.abc7447
- Castaña, C., Camarero, J. J., Zas, R., Sampedro, L., Bonet, J. A., Alday, J. G., et al. (2020). Insect defoliation is linked to a decrease in soil ectomycorrhizal biomass and shifts in needle endophytic communities. *Tree Physiol.* 40, 1712–1725. doi: 10.1093/treephys/tpaa104
- Cook, E. R., and Krusic, P. (2007). *ARSTAN 44 A Tree-ring standardization program based on detrending and autoregressive time series modeling with interactive graphics*. Available at: <https://www.geog.cam.ac.uk/research/projects/dendrosoftware/> (Accessed 8 March 2023).
- Démolin, G. (1969). Bioecología de la “procesionaria del pino” *Thaumetopoea pityocampa* Schiff. Incidencia de los factores climáticos. *Bol. Serv. Plagas For.* 23, 9–24.
- DeSoto, L., de la Cruz, M., and Fonti, P. (2011). Intra-annual pattern of tracheid size in the Mediterranean *JuniPerus thurifera* as indicator for seasonal water stress. *Can. J. For. Res.* 41, 1280–1294. doi: 10.1139/x11-045
- Donaldson, L. A. (2002). Abnormal lignin distribution in wood from severely drought stressed *Pinus radiata* trees. *IAWA J.* 23, 161–178. doi: 10.1163/22941932-90000295
- Ferrio, J. P., and Voltas, J. (2005). Carbon and oxygen isotope ratios in wood constituents of *Pinus halepensis* as indicators of precipitation, temperature and vapour pressure deficit. *Tellus B.* 57, 164–173. doi: 10.3402/tellusb.v57i2.16780
- Forkel, M., Carvalhais, N., Verbesselt, J., Mahecha, M., Neigh, C., and Reichstein, M. (2013). Trend change detection in NDVI time series: effects of inter-annual variability and methodology. *Remote Sens.* 5, 2113–2144. doi: 10.3390/rs5052113
- Fritts, H. C. (1976). *Tree rings and climate* (London: Academic Press).

- Gärtner, H., and Nievergelt, D. (2010). The core-microtome. A new tool for surface preparation on cores and time series analysis of varying cell parameters. *Dendrochronologia* 28, 85–92. doi: 10.1016/j.dendro.2009.09.002
- Gazol, A., Hernández-Alonso, R., and Camarero, J. J. (2019). Patterns and drivers of pine processionary moth defoliation in Mediterranean mountain forests. *Front. Ecol. Evol.* 28. doi: 10.3389/fevo.2019.00458
- Gierlinger, N. (2014). Revealing changes in molecular composition of plant cell walls on the micron-level by Raman mapping and vertex component analysis (VCA). *Front. Plant Sci.* 5. doi: 10.3389/fpls.2014.00306
- Gierlinger, N., Kepling, T., and Harrington, M. (2012). Imaging of plant cell walls by confocal Raman microscopy. *Nat. Prot.* 7, 1694–1708. doi: 10.1038/nprot.2012.092
- Gross, H. L. (1992). Impact analysis for a jack pine budworm infestation in Ontario. *Can. J. For. Res.* 22, 818–831. doi: 10.1139/x92-111
- Güney, A. (2019). “Effects of defoliation caused by pine processionary moth on xylem anatomy in Turkish pine,” in *4th Xylem International Meeting*, Padua, Italy, 25–27 September 2019.
- Hänninen, T., Kontturi, E., and Vuorinen, T. (2011). Distribution of lignin and its coniferyl alcohol and coniferyl aldehyde groups in *Picea abies* and *Pinus sylvestris* as observed by Raman imaging. *Phytochemistry* 72, 1889–1895. doi: 10.1016/j.phytochem.2011.05.005
- Hantson, S., and Chuvieco, E. (2011). Evaluation of different topographic correction methods for Landsat imagery. *Int. J. Appl. Earth Obs. Geoinf.* 13, 691–700. doi: 10.1016/j.jag.2011.05.001
- Harvey, J. A., Heinen, R., Gols, R., and Thakur, M. P. (2020). Climate change-mediated temperature extremes and insects: from outbreaks to breakdowns. *Glob. Change Biol.* 26, 6685–6701. doi: 10.1111/gcb.15377
- Hernández Alonso, R., Pérez Fortea, V., Camarero, J. J., Montoya, R., and Sánchez Peña, G. (2005). “Efectos de la defoliación inducida por la procesionaria del pino (*Thaumetopoea pityocampa*) sobre el crecimiento y la supervivencia de *Pinus nigra* e interacciones con el clima durante el período 1992–2004,” in *Actas del IV Congreso Forestal Español* (Zaragoza, Spain), 366–374.
- Hódar, J. A., Castro, J., and Zamora, R. (2003). Pine processionary caterpillar *Thaumetopoea pityocampa* as a new threat for relict Mediterranean Scots pine forests under climatic warming. *Biol. Conserv.* 110, 123–129. doi: 10.1016/S0006-3207(02)00183-0
- Hódar, J. A., Zamora, R., Castro, J., and Baraza, E. (2004). Feast and famine: previous defoliation limiting survival of pine processionary caterpillar *Thaumetopoea pityocampa* in Scots pine *Pinus sylvestris*. *Acta Oecol.* 26, 203–210. doi: 10.1016/j.actao.2004.05.004
- Holmes, R. L. (1983). Computer-assisted quality control in tree-ring dating and measurement. *Tree-Ring Bull.* 43, 69–75.
- Hunt, E. R., and Rock, B. N. (1989). Detection of changes in leaf water content using near and middle-infrared reflectances. *Rem. Sens. Env.* 30, 43–54. doi: 10.1016/0034-4257(89)90046-1
- Jacquet, J.-S., Oracio, C., and Jactel, H. (2012). Defoliation by processionary moth significantly reduces tree growth: a quantitative review. *Ann. For. Sci.* 69, 857–866. doi: 10.1007/s13595-012-0209-0
- Jactel, H., Petit, J., Desprez-Loustau, M. L., Delzon, S., Piou, D., Battisti, A., et al. (2012). Drought effects on damage by forest insects and pathogens: a meta-analysis. *Glob. Change Biol.* 18, 267–276. doi: 10.1111/j.1365-2486.2011.02512.x
- Kanat, M., Hakki, M. A., and Sivrikaya, F. (2005). Effect of defoliation by *Thaumetopoea pityocampa* (Den. & Schiff.) (Lepidoptera: Thaumetopoeidae) on annual diameter increment of *Pinus brutia* Ten. *Ann. For. Sci.* 62, 91–94. doi: 10.1051/forest:2004095
- Kulman, H. M. (1971). Effects of insect defoliation on growth and mortality of trees. *Ann. Rev. Entomol.* 16, 289–324. doi: 10.1146/annurev.en.16.010171.001445
- Linares, J. C., Senhadja, K., Herrero, A., and Hódar, J. A. (2014). Growth patterns at the southern range edge of Scots pine: Disentangling the effects of drought and defoliation by the pine processionary caterpillar. *For. Ecol. Manage.* 315, 129–137. doi: 10.1016/j.foreco.2013.12.029
- Loader, N. J., Robertson, I., Barker, A. C., Switsur, V. R., and Waterhouse, J. S. (1997). An improved technique for the batch processing of small whole wood samples to alpha-cellulose. *Chem. Geol.* 136, 313–317. doi: 10.1016/S0009-2541(96)00133-7
- Lynch, A. M. (2012). “What tree ring reconstructions tell us about conifer defoliation outbreaks,” in *Insect Outbreaks Revisited*. Eds. P. Barbosa, D. K. Letourneau and A. A. Agrawal (Hoboken, USA: Blackwell), 126–154.
- Millar, C. I., and Stephenson, N. L. (2015). Temperate forest health in an era of emerging megadisturbance. *Science* 349, 823–826. doi: 10.1126/science.aaa9933
- Montoya, R., and Hernández, R. (1991). “La procesionaria del pino,” in *Plagas de Insectos en las Masas Forestales Españolas*. Eds. N. Romanyk and D. Cadahia (Madrid, Spain: Ministerio de Agricultura, Pesca y Alimentación), 59–73.
- Navarro, L., Hubert, M., Bergeron, Y., and Montoro Girona, M. (2018). Changes in spatiotemporal patterns of 20th century spruce budworm outbreaks in eastern Canadian boreal forests. *Front. Plant Sci.* 9, 1905. doi: 10.3389/fpls.2018.01905
- Palacio, S., Hernández, R., Maestro-Martínez, M., and Camarero, J. J. (2012). Fast replenishment of initial carbon stores after defoliation by the pine processionary moth and its relationship to the re-growth ability of trees. *Trees Struct. Funct.* 26, 1627–1640. doi: 10.1007/s00468-012-0739-y
- Paritsis, J., Veblen, T. T., and Kitzberger, T. (2009). Assessing dendroecological methods to reconstruct defoliator outbreaks on *Nothofagus pumilio* in northwestern Patagonia, Argentina. *Can. J. For. Res.* 39, 1617–1629. doi: 10.1139/X09-085
- Polge, H., and Garros, S. (1971). Influence de défoliations sur la structure du bois de pin maritime. *Ann. Sci. For.* 28, 195–206. doi: 10.1051/forest/19710204
- Prendin, A. L., Carrer, M., Karami, M., Hollesen, J., Pedersen, N. B., Pividori, M., et al. (2020). Immediate and carry-over effects of insect outbreaks on vegetation growth in West Greenland assessed from cells to satellite. *J. Biogeogr.* 47, 87–100. doi: 10.1111/jbi.13644
- Prendin, A. L., Carrer, M., Pedersen, N. B., Normand, S., Hollesen, J., Treier, U. A., et al. (2021). Chemical signature of *Eurois occulta* L. outbreaks in the xylem cell wall of *Salix glauca* L. outbreaks in Greenland. *Sci. Tot. Env.* 764, 144607. doi: 10.1016/j.scitotenv.2020.144607
- Proe, M. F., Midwood, A. J., and Craig, J. (2000). Use of stable isotopes to quantify nitrogen, potassium and magnesium dynamics in young Scots pine (*Pinus sylvestris*). *New Phytol.* 146, 461–469. doi: 10.1046/j.1469-8137.2000.00658.x
- R Development Core Team (2022). *R: A language and environment for statistical computing* (Vienna, Austria: R Foundation for Statistical Computing). Available at: <http://www.R-project.org/>.
- Régolini, M., Castagneyrol, B., Dulaurent-Mercadal, A.-M., Piou, D., Samalens, J.-C., and Jactel, H. (2014). Effect of host tree density and apparency on the probability of attack by the pine processionary moth. *For. Ecol. Manage.* 334, 185–192. doi: 10.1016/j.foreco.2014.08.038
- Roden, J. S., and Farquhar, G. D. (2012). A controlled test of the dual-isotope approach for the interpretation of stable carbon and oxygen isotope ratio variation in tree rings. *Tree Physiol.* 32, 490–503. doi: 10.1093/treephys/tps019
- Roques, A., Rousset, J., Avc, M., Avtzis, D., Basso, A., Battisti, A., et al. (2015). “Climate warming and past and present distribution of the processionary moths (*Thaumetopoea*) in Europe, Asia Minor and North Africa,” in *Processionary Moths and Climate Change: An Update*. Ed. A. Roques (Dordrecht: Springer), 81–161.
- Roy, D. P., Kovalsky, V., Zhang, H. K., Vermote, E. F., Yan, L., Kumar, S. S., et al. (2016). Characterization of Landsat-7 to Landsat-8 reflective wavelength and normalized difference vegetation index continuity. *Rem. Sens. Env.* 185, 57–70. doi: 10.1016/j.rse.2015.12.024
- Sangüesa-Barreda, G., Camarero, J. J., García-Martín, A., Hernández, R., and de la Riva, J. (2014). Remote-sensing and tree-ring based characterization of forest defoliation and growth loss due to the Mediterranean pine processionary moth. *For. Ecol. Manage.* 320, 171–181. doi: 10.1016/j.foreco.2014.03.008
- Scheidegger, Y., Saurer, M., Bahn, M., and Siegwolf, R. (2000). Linking stable oxygen and carbon isotopes with stomatal conductance and photosynthetic capacity: a conceptual model. *Oecologia* 125, 350–357. doi: 10.1007/s004420000466
- Schneider, C. A., Rasband, W. S., and Eliceiri, K. W. (2012). NIH Image to ImageJ: 25 years of image analysis. *Nat. Methods* 9, 671–675. doi: 10.1038/nmeth.2089
- Shestakova, T. A., Camarero, J. J., Ferrio, J. P., Knorr, A. A., Gutiérrez, E., and Voltas, J. (2017). Increasing drought effects on five European pines modulate $\Delta^{13}\text{C}$ -growth coupling along a Mediterranean altitudinal gradient. *Funct. Ecol.* 31, 1359–1370. doi: 10.1111/1365-2435.12857
- Simler-Williamson, A. B., Rizzo, D. M., and Cobb, R. C. (2019). Interacting effects of global change on forest pest and pathogen dynamics. *Ann. Rev. Ecol. Evol. Syst.* 50, 381–403. doi: 10.1146/annurev-ecolsys-110218-024934
- Speer, J. H., Swetnam, T. W., Wickman, B. E., and Youngblood, A. (2001). Changes in Pandora moth outbreak dynamics during the past 622 years. *Ecology* 82, 670–697. doi: 10.1890/0012-9658(2001)082[0679:CIPMOD]2.0.CO;2
- Sutton, A., and Tardif, J. C. (2005). Distribution and anatomical characteristics of white rings in *Populus tremuloides*. *IAWA J.* 26, 221–238.
- Swetnam, T. W., and Lynch, A. M. (1993). Multicentury, regional-scale patterns of western spruce budworm outbreaks. *Ecol. Monogr.* 63, 399–424. doi: 10.2307/2937153
- Swetnam, T. W., Thompson, M. A., and Sutherland, E. K. (1985). *Using dendrochronology to measure radial growth of defoliated trees* Vol. 639 (Washington, DC, USA: US Forest Service).
- Tucker, C. (1979). Red and photographic infrared linear combinations for monitoring vegetation. *Rem. Sens. Env.* 8, 127–150. doi: 10.1016/0034-4257(79)90013-0
- Vaganov, E. A., Hughes, M. K., and Shashkin, A. K. (2006). *Growth Dynamics of Conifer Tree Rings Images of Past and Future Environments* (Berlin: Springer).
- Verbesselt, J., Zeileis, A., and Herold, M. (2012). Near real-time disturbance detection using satellite image time series. *Rem. Sens. Env.* 123, 98–108. doi: 10.1016/j.rse.2012.02.022
- Vicente-Serrano, S. M., Tomás-Burguera, M., Beguería, S., Reig-Gracia, F., Latorre, B., Peña-Gallardo, M., et al. (2017). A high resolution dataset of meteorological drought indices for Spain. *Data* 2, 22. doi: 10.3390/data2030022
- Voltas, J., Camarero, J. J., Carulla, D., Aguilera, M., Oriz, A., and Ferrio, J. P. (2013). A retrospective, dual-isotope approach reveals individual predispositions to winter-drought induced tree dieback in the southernmost distribution limit of Scots pine. *Plant Cell Env.* 36, 1435–1448. doi: 10.1111/pce.12072

Von Wilpert, K. (1991). Intraannual variation of radial tracheid diameters as monitor of site specific water stress. *Dendrochronologia* 9, 95–113.

Warren, C. R. (2006). Why does photosynthesis decrease with needle age in *Pinus pinaster*? *Trees Struct. - Funct.* 20, 157–164. doi 10.1007/s00468-005-0021-7

Wyka, T. P., Żytkowiak, R., and Oleksyn, J. (2016). Seasonal dynamics of nitrogen level and gas exchange in different cohorts of Scots pine needles: a conflict between nitrogen mobilization and photosynthesis? *Eur. J. For. Res.* 135, 483–493. doi: 10.1007/s10342-016-0947-x